MOX-Report No. 54/2016

Large Eddy Simulations of blood dynamics in abdominal aortic aneurysms

Vergara, C.; Le Van, D.; Quadrio, M.; Formaggia, L.; Domanin, M.

MOX, Dipartimento di Matematica
Politecnico di Milano, Via Bonardi 9 - 20133 Milano (Italy)

mox-dmat@polimi.it http://mox.polimi.it

Large Eddy Simulations of blood dynamics in abdominal aortic aneurysms*

C. Vergara[1], D. Le Van[1], M. Quadrio[2], L. Formaggia[1], M. Domanin[3]

December 13, 2016

[1] MOX– Modellistica e Calcolo Scientifico
Dipartimento di Matematica
Politecnico di Milano
<christian.vergara,luca.formaggia>@polimi.it, davide.le@mail.polimi.it

[2] Dipartimento di Scienze e Tecnologie Aerospaziali
Politecnico di Milano, Italy maurizio.quadrio@polimi.it

[3] Operative Unit of Vascular Surgery, Fondazione I.R.C.C.S. Ca' Granda Ospedale Maggiore Policlinico di Milano, Italy and Department of Clinical Sciences and Community, Universitá di Milano, Italy maurizio.domanin@unimi.it

Abstract

In this work we address the study of transition to turbulence effects in abdominal aortic aneurysms (AAA). The formation of transitional effects in such districts is caused by the heart pulsatility and the sudden change of diameter, and has been recorded by means of clinical measures and computational studies. Here we propose, for the first time, the use of a large eddy simulation (LES) model to describe transition to turbulence in realistic scenarios of AAA obtained from radiological images. To this aim, we post-process the obtained numerical solutions to produce significant quantities, such as the ensemble-averaged velocity and wall shear stress, the standard deviation of the velocity field, the Q-criterion. The results show the suitability of the considered LES model and the presence of significant transitional effects during the mid-deceleration phase around the impingement region.

Keywords: Abdominal aortic aneurysm, large eddy simulation, ensemble-average, transition to turbulence

*CV and LF have been partially supported by the Italian MIUR PRIN12 project no. 201289A4LX "Modelli matematici e numerici del sistema cardiocircolatorio e loro applicazione in ambito clinico". DLV has been supported by the ERC 2015 Proof of Concept "math4AAArisk" (A mathematical platform for Abdominal Aortic Aneurism risk assessment and surgical planning).

1 Introduction

Blood fluid-dynamics plays a major role in the development of abdominal aortic aneurysms (AAA), i.e. the enlargement of the abdominal aorta whose rupture could lead to fatal events [14]. In particular, specific wall shear stress (WSS) conditions regulate the production of the nitric oxide [3], which is known to determine the loss of elastin at the basis of the aneurysm formation and growth; determine the activation of blood platelets [34], playing a central role in the thrombus formation; and are responsible for anisotropic displacements of the aneurysmatic sac [37].

In this context, the possibility for the flow regime to be transitional or turbulent owing to the enlargement of the lumen and to pulsatility [5, 12] have a strong impact on WSS and thus on the above-mentioned relationships. In particular, turbulence effects are responsible for an increased platelets activation [10] and damage of the blood cell [49], and provide additional stresses that may lead to further AAA dilatation [27]. Although not mainly determined by WSS, also the rupture process may be influenced by turbulence in the aneurysm, since the corresponding arterial wall vibration may damage the structural components of the wall [2].

For these reasons, the inclusion of turbulence models (or the use of well-resolved meshes) is mandatory for a computational study of blood dynamics in AAA and for an accurate description of the anurysm evolution [2, 27, 30]. One major issue relies on the qualification and quantification of turbulence, since its very definition is quite problematic in general and in particular in hemodynamics. Indeed, in this context turbulence does not fully develop since the acceleration at the beginning of a new heartbeat laminarizes the flow which experiences only a transitional behavior [49]. This is a common fact in vascular hemodynamics, see for example [44, 21, 29, 40] for the case of stenotic carotids. Often, with turbulence some authors meant the presence of disturbed and/or vorticous blood flows. Only few computational studies have introduced suitable statistically-based quantities to assess turbulence effects in AAA [2, 30].

In this work, we consider *large eddy simulations* (LES) for the study of transition to turbulence effects in AAA. In particular, we apply the eddy-viscosity $\sigma-$model [33] to three patient-specific geometries. To assess turbulence effects, we study the standard deviation of the velocity field, the ratio between eddy and molecular viscosities, and the fluctuations of the kinetic energy. Our results show the suitability of LES models in hemodynamics and the presence of a significant amount of transitional effects localized close to the jet impingement region during the deceleration phase.

2 Materials and Methods

2.1 Geometric data

Three patients (P1, P2, and P3 in what follows) who underwent 4D-CT as preoperative evaluation of an AAA were selected and approved ethical review board approval and informed consent. The radiological acquisitions were performed with a Somatom Definition Dual Source CT (Siemens, Erlangen, Germany), before and after contrast media administration with retrospectively electrocardiographic (ECG) gated spiral acquisition. Non-ionic contrast media (Iomeron, Bracco, Milan, Italy) was used.

The 3D geometric reconstructions were performed by means of the Vascular Modeling Toolkit, VMTK [1]. The 3D surface model of the lumen surface of the abdominal aorta was reconstructed using a gradient-driven level set technique. Then, the surface models of the three geometries were turned into volumetric meshes of linear tetrahedra, with three thin layers close to the wall. In particular, the meshes were formed by 275k and 110k tetrahedra for P1, 115k tetraedra for P2, and 120k tetraedra for P3. These values correspond to a characteristic space discretization parameter $h = 0.08\,cm$ and $h = 0.11\,cm$ for P1, and $h = 0.13\,cm$ for P2 and P3.

2.2 Numerical methods

Blood is modelled as a constant density, Newtonian and homogeneous fluid, a well accepted hypothesis for medium and large vessels [16].

LES models are based on the decomposition of the fluid unknowns in resolved and unresolved quantities, $[\overline{\boldsymbol{u}}, \overline{p}]$ and $[\boldsymbol{u}', p']$, respectively, so that $\boldsymbol{u} = \overline{\boldsymbol{u}} + \boldsymbol{u}'$ and $p = \overline{p} + p'$ [41]. The resolved quantities are referred to as *filtered*. In order to derive a set of equations for $\overline{\boldsymbol{u}}$ and $\overline{p}$, a formal filtering procedure is performed over the Navier-Stokes equations. Defining $\boldsymbol{\tau} = \overline{\boldsymbol{u} \otimes \boldsymbol{u}} - \overline{\boldsymbol{u}} \otimes \overline{\boldsymbol{u}}$ the *subgrid-scale* tensor, which models the effect of the unresolved scales on the resolved ones [43, 38], we consider the following filtered Navier-Stokes problem (normalized over the fluid density):
Find the velocity $\overline{\boldsymbol{u}}(t, \boldsymbol{x})$ and the pressure $\overline{p}(t, \boldsymbol{x})$ such that

$$\frac{\partial \overline{\boldsymbol{u}}}{\partial t} - \nu \nabla \cdot \boldsymbol{S}(\overline{\boldsymbol{u}}) + \nabla \cdot (\overline{\boldsymbol{u}} \otimes \overline{\boldsymbol{u}}) + \nabla \overline{p} + \nabla \cdot \boldsymbol{\tau}^d(\overline{\boldsymbol{u}}) = \boldsymbol{0} \qquad t \in (0, MT],\ \boldsymbol{x} \in \Omega, \tag{1a}$$

$$\nabla \cdot \overline{\boldsymbol{u}} = 0 \qquad t \in (0, MT],\ \boldsymbol{x} \in \Omega, \tag{1b}$$

$$\overline{\boldsymbol{u}} = \boldsymbol{g} \qquad t \in (0, MT],\ \boldsymbol{x} \in \Gamma_{in}, \tag{1c}$$

$$-\overline{p}\boldsymbol{n} + \nu \boldsymbol{S}(\overline{\boldsymbol{u}})\boldsymbol{n} - \boldsymbol{\tau}^d(\overline{\boldsymbol{u}})\boldsymbol{n} = \boldsymbol{0} \qquad t \in (0, MT],\ \boldsymbol{x} \in \Gamma_{out}, \tag{1d}$$

with zero initial boundary condition for the velocity, and where M is the number of heartbeats, T the period of a heartbeat, $(\boldsymbol{u} \otimes \boldsymbol{u})_{ij} = u_i u_j$, $\boldsymbol{S}(\boldsymbol{u}) = \nabla \boldsymbol{u} + (\nabla \boldsymbol{u})^T$, Γ_{in} is the inlet, Γ_{out} the two outlets given by the iliac segments, ν is the kinematic viscosity, and $\boldsymbol{g}(t, \boldsymbol{x})$ is a given boundary data. In particular, at the inlet Γ_{in} we impose a representative time variation of the flow rate $Q(t)$ reported in Figure 1. Here the flow rate is defined as

$$Q = \int_{\Gamma_{in}} \overline{\boldsymbol{u}} \cdot \boldsymbol{n} \, d\sigma. \tag{2}$$

This is a defective boundary condition, since at each time step we are prescribing only a scalar quantity over the whole Γ_{in}. In order to fill this gap, we make the assumption of parabolic velocity profile along the normal direction, yielding the Dirichlet condition (1c), $\boldsymbol{g}$ being the unique function with a parabolic profile in the normal direction and vanishing in the tangential ones, with flow rate at each time step equal to $Q(t)$. No perturbation is prescribed, so that the flow is assumed to be laminar at the inlet boundary. This will allow us to capture transitional effects arising as a consequence of geometry and pulsatility solely.

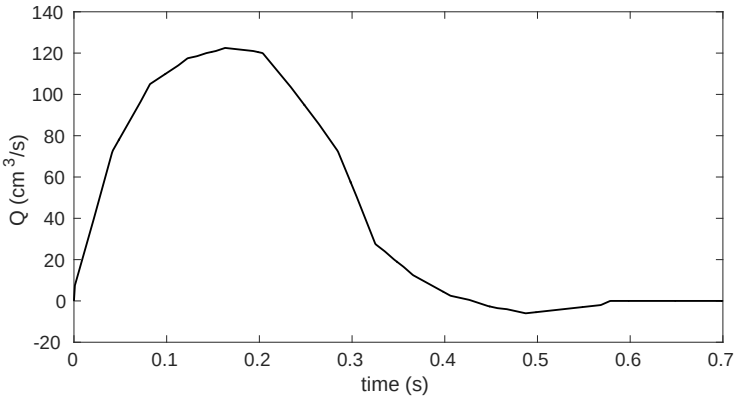

Figure 1: Flow waveform prescribed at the inlet.

The tensor $\boldsymbol{\tau}^d = \boldsymbol{\tau} - \frac{1}{3}\sum_k \tau_{kk} \boldsymbol{I}$ in (1) is the deviatoric part of the subgrid-scale tensor $\boldsymbol{\tau}$. The latter is suitably modeled as a function of the filtered quantities $\overline{\boldsymbol{u}}$, hence equations (1) have only $(\overline{\boldsymbol{u}}, \overline{p})$ as dependent variables. Usually, the effect of the subgrid-scale on the resolved scales is modeled in analogy with the kinetic theory of gases, by introducing a subgrid-scale viscosity ν_{sgs} and by modeling the deviatoric part of the subgrid-scale tensor as follows

$$\boldsymbol{\tau}^d(\overline{\boldsymbol{u}}) = -2\nu_{sgs}(\overline{\boldsymbol{u}}) \boldsymbol{S}(\overline{\boldsymbol{u}}).$$

The eddy viscosity model considered in this work is the $\sigma-$model, introduced in [33]. This is based on the introduction of the singular values $\sigma_1(t, \boldsymbol{x}) \geq \sigma_2(t, \boldsymbol{x}) \geq$

$\sigma_3(t, \boldsymbol{x}) \geq 0$ of $\nabla \overline{\boldsymbol{u}}$, and on defining the subgrid-scale viscosity as follows:

$$\nu_{sgs} = C\overline{\Delta}^2 \frac{\sigma_3(\sigma_1 - \sigma_2)(\sigma_2 - \sigma_3)}{\sigma_1^2}, \tag{3}$$

where C is a suitable constant and $\overline{\Delta}$ the filter width. In our simulation we set $C = 1.5$ [33, 28]. For the grid filter we considered an *implicit* procedure [11], where the filter width $\overline{\Delta}$ represents the size of a mesh that is not able to capture all the scales [38]. This empirical choice is the most widely used today.

As for the time discretization, we use a semi-implicit approach to linearize the momentum equation (1a), used in combination with a BDF2 scheme [22]. In particular, the convective field and the subgrid-scale viscosity have been evaluated by means of a second order extrapolation [28]. This treatment yields a CFL-like limitation on the time step Δt ($\Delta t \lesssim h$, see [39]). For the space discretization we use Finite Elements with a SUPG stabilization term added to control numerical instabilities due to the large convective term [46]. We used $P2 - P2$ Finite Elements, that is piecewise quadratic polynomials for the approximation of the pressure and each velocity component. A Pressure Stabilized Petrov-Galerkin (PSPG) formulation [46] was used to ensure the non-singularity of the corresponding matrix. For the description of the complete discretized-in-time problem, we refer the reader to [28].

We use the following data: physical viscosity $\nu = 0.033\, cm^2/s$, $\Delta t = 0.001\, s$, $M = 6$, $T = 0.7\, s$.

All numerical results have been obtained using the parallel Finite Element library `LIFEV` (`www.lfev.org`).

2.3 Quantities of interest

To describe the blood dynamics and in particular transitional effect in the three AAA geometries, we introduce the following post-processed quantities:

- *Ensemble-average.* Given a quantity $S(\boldsymbol{x})$, we define its ensemble-average the quantity

$$< S(t, \boldsymbol{x}) >= \frac{1}{M} \sum_{j=1}^{M} S(t + (j-1)T), \qquad t \in (0, T],\, \boldsymbol{x} \in \Omega.$$

  This will allow us to eliminate from the field of interest the random fluctuactions due to the transitional effects appearing at each heartbeat. In this study, we consider the ensemble-average velocity magnitude $< U >$ and wall shear stress $< WSS >$, where

$$U(t, \boldsymbol{x}) = \|\overline{\boldsymbol{u}}(t, \boldsymbol{x})\|_{\mathbb{R}^3} \qquad WSS(t, \boldsymbol{x}) = \nu \sqrt{\sum_{j=1}^{2} \left(\nabla \overline{\boldsymbol{u}}\, \boldsymbol{n}\right) \cdot \boldsymbol{\tau}^{(j)}\Big)^2}, \qquad t \in (0, MT],\, \boldsymbol{x} \in \Omega,$$

where the latter quantity is computed on the lateral surface, $\boldsymbol{n}$ is the outward unit vector, and $\boldsymbol{\tau}^{(j)}$, $j = 1, 2$, the tangential unit vectors;

- *Standard deviation of the velocity magnitude.* At each point $\boldsymbol{x}$, this is defined as usual as

$$SD(t, \boldsymbol{x}) = \sqrt{\frac{1}{M}\sum_{j=1}^{M} \left(U(t + (j-1)T, \boldsymbol{x}) - < U(t, \boldsymbol{x}) >\right)^2}, \ t \in (0, T], \ \boldsymbol{x} \in \Omega.$$

  This will allow us to quantify and localize the velocity fluctuations among the heartbeats;

- *Q-criterion.* It is defined as

$$Q(t, \boldsymbol{x}) = -\frac{1}{2}\left(\sum_{i,j} S_{ij}^2(t, \boldsymbol{x}) - \Omega_{ij}^2(t, \boldsymbol{x})\right), \quad t \in (0, MT], \ \boldsymbol{x} \in \Omega,$$

  where $\boldsymbol{\Omega} = \nabla\overline{\boldsymbol{u}} - (\nabla\overline{\boldsymbol{u}})^T$ [9, 29]. Positive values of Q indicate locations where rotations dominates strain and shear. This will allow us to identify regions where vortical structures are present;

- *Global Turbulent Kinetic Energy (TKE).* It is defined as the space average of the Turbulent Kinetic Energy [30]:

$$k(t) = \frac{1}{2}\int_\Omega \frac{1}{M}\sum_{j=1}^{M} \Big((\overline{u}_x(t + (j-1)T, \boldsymbol{x}) - < u_x(t, \boldsymbol{x}) >)^2 +$$

$$(\overline{u}_y(t + (j-1)T, \boldsymbol{x}) - < u_y(t, \boldsymbol{x}) >)^2 +$$

$$(\overline{u}_z(t + (j-1)T, \boldsymbol{x}) - < u_z(t, \boldsymbol{x}) >)^2 \Big) \, d\boldsymbol{x}, \quad t \in (0, T].$$

  TKE is representative of the cycle-to-cycle variation of the velocity field and its average-in-space values defined above will allow us to identify the temporal instants within the heartbeat where fluctuations in the whole AAA are more pronounced. Moreover, the average and maximum in time k_{mean} and k_{max}, respectively, of $k(t)$ are proposed in this study as synthetic indices to quantify the amount of variability of the velocity field in the aneurysmatic sac and thus possible transitional effects.

3 Results

3.1 Assessment of the computational meshes

The goal of LES models consists in accurately describing turbulent flows on a mesh that is coarser than the one needed to perform a Direct Numerical

Simulation (DNS). Thus, a suitable mesh to be used with a LES model should be neither too fine, in order to be a valid alternative to DNS, nor too coarse, such that the modelling assumptions remain valid. To this aim, in this first set of simulations, we compare the results obtained for P1 with two meshes in order to estimate the number of tetrahedra of a reasonable mesh.

Referring to the results reported in Figure 2, we first observe that, as expected, blood flow is characterized by a jet that impinges on the distal part of the aneurysmatic sac (see figures at the top, where the ensemble-averaged velocity magnitude $< U >$ has been plotted). Secondly, we observe an excellent qualitative agreement between $< U >$ computed in the two meshes. This suggests that the coarser mesh is suitable for our purposes. This is also confirmed by the ratio between the subgrid-scale and molecular viscosities, reported in Figure 2, bottom. These figures clearly indicate the presence of transitional effects in the aneurismatic sac, in particular at the mid-deceleration and early diastolic phases. The subgrid-scale viscosity reaches values up to five times the molecular one in the coarsest mesh and up to 3 times in the finest one. This means that the contribution of the subgrid-scale modeling is, as expected, greater for the coarsest mesh in order to account for the higher frequency cutoff introduced in this case by the implicit filter. At the same time, the numerical errors introduced by the coarsest mesh are still not relevant enough to compromise the accuracy, since the results are in accordance with the finest mesh. For all these reasons, in what follows for P2 and P3 we consider meshes of the same refinement degree of the coarsest one used for P1.

3.2 Description of transitional effects

In Figure 3 we report for P2 and P3 the same quantities plotted in Figure 2 for P1, that is the ensemble-averaged velocity magnitude and the ratio between the subgrid-scale and molecular viscosities. From these figures we observe again the jet impingement in the distal region of the aneurysmatic sac of P2. Instead, for P3 the non-axiality of the the tract of the aorta just above the sac forces the jet to impinge on the proximal part of the sac. Moreover, we observe that, as for P1, for both P2 and P3 the LES model is active, in particular during the mid-deceleration and early diastolic phases, with the subgrid-scale viscosity reaching values up to five times greater than those of the molecular viscosity.

In Figure 4, left, we report for all three cases the values of the standard deviation of the velocity magnitude at the same three time instants of above. These plots show high values of the standard deviation for all the three cases at the early diastole and for P1 and P3 also at the mid-deceleration phase. These values are of the same order of magnitude of the velocity itself (look at Figures 2 and 3). In the same figure, on the right, we plot vortical structures identified by means of the Q-criterion, that highlights the formation of a vortex ring at the systolic peak, which impinges the aneurysmatic sac at the mid-deceleration phase and, after the breakage, partially exits through the iliac outlets.

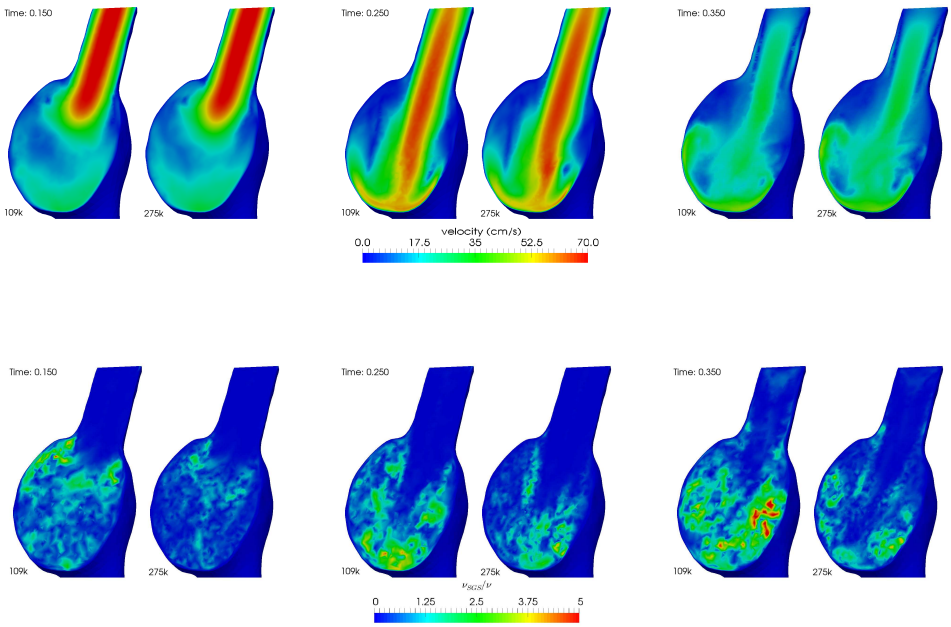

Figure 2: Top: Ensemble-averaged velocity magnitude; Bottom: Ratio between the subgrid-scale and molecular viscosities. In each figure, we report on the left the results obtained with the coarse mesh and on the right those obtained with the fine mesh. Three time instants are reported: Systolic peak instant $t = 0.15\,s$ (left); Mid-deceleration $t = 0.25\,s$ (middle); Early diastole $t = 0.35\,s$ (right).

In Figure 5 we report the time evolution of the global Kinetic Turbulent Energy for the three patients. We observe that for all the cases, the peak value is reached during the mid-deceleration phase ($t \simeq 0.3 - 0.4\,s$). Moreover, we observe significant lower values for P2 with respect to P1 and P3, confirmed also by the mean and maximum in time values reported in Table 1, where we report also the dimensions of the three AAA.

	P1	P2	P3
CC length	4.9	4.9	6.9
AP diameter	4.5	4.1	3.9
LL diameter	4.5	3.9	4.8
k_{mean}	19.0	13.2	21.0
k_{max}	46.8	32.1	47.2

Table 1: Values of the craniocaudal length (from the neck to the iliac outlets, in cm), of the antero-posterior and latero-lateral diameters (in cm), and of the mean and maximum in time of $k(t)$ (in cm^2/s^2).

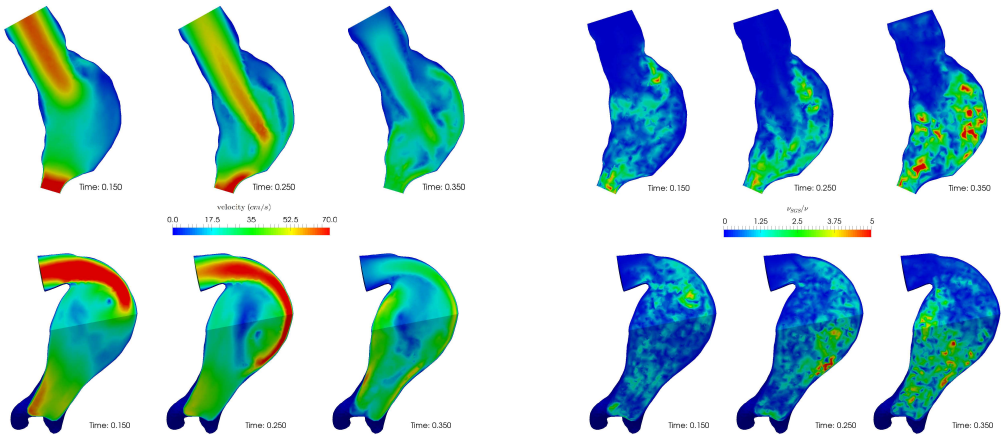

Figure 3: Left: Ensemble-averaged velocity magnitude; Right: Ratio between the subgrid-scale and molecular viscosities. Top: Results for P2; Bottom: Results for P3. Three time instants are reported: Systolic peak instant $t = 0.15\,s$ (left); Mid-deceleration $t = 0.25\,s$ (middle); Early diastole $t = 0.35\,s$ (right).

The peak systolic Reynolds number for all the cases is computed as

$$Re = \frac{V_{sist} D}{\nu} = \frac{4 Q_{sist}}{\pi D \nu} \simeq 2200,$$

where V_{sist} is the mean systolic velocity at the inlet, $Q_{sist} = 120\,cm^3/s$ the systolic flow rate prescribed at the inlet (see Figure 1), and $D \simeq 2\,cm$ a representative value, for all the patients, of the diameter at the inlet.

Last, in Figure 6 we report the spatial distribution of the ensemble-averaged WSS at the time instant where it reaches its maximum value ($t = 0.3\,s$). From this figure, we observe large values in correspondance of the impingement regions.

4 Discussion

4.1 The presence of turbulence in abdominal aortic aneurysms and its clinical implications

The presence of turbulence in healthy vascular vessels seems to be confined to the ascending and thoracic aorta. However, these effects are quite negligible since, in physiological conditions, the helicity developed in such districts as a consequence of the ventricular contraction reduces the turbulent kinetic energy [32]. A different situation occurs in pathological districts, where significant transition to turbulence effects could develop, often as a consequence of a change of the geometry. For example, this is the case of stenotic carotids [44, 4, 45, 21, 29, 13, 7, 40].

Turbulence effects in abdominal aortic aneurysms due to the sudden change of geometric shape and to pulsatility have been observed in-vivo by means of

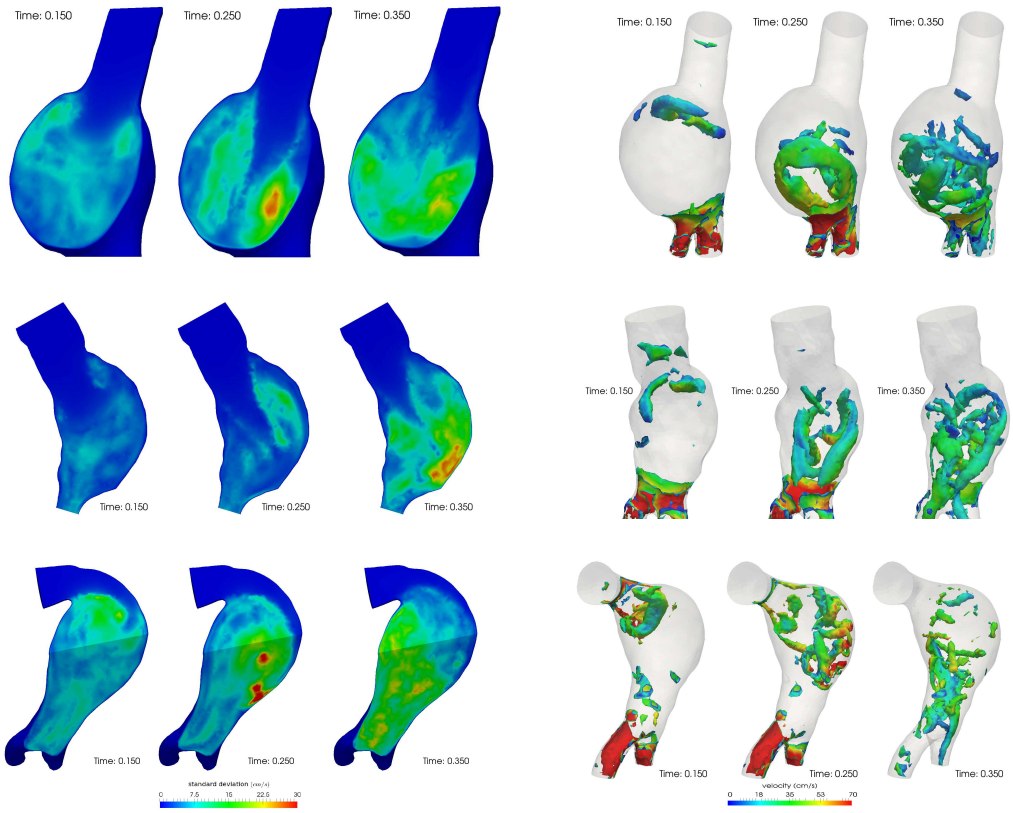

Figure 4: Left: Standard deviation of the velocity magnitude. Right: Q-criterion (we report the regions with $Q > 5000$ painted by the velocity magnitude). Top: Results for P1; Middle: Results for P2; Bottom: Results for P3. Three time instants are reported for each case: Systolic peak instant $t = 0.15\,s$; Mid-deceleration $t = 0.25\,s$; Early diastole $t = 0.35\,s$.

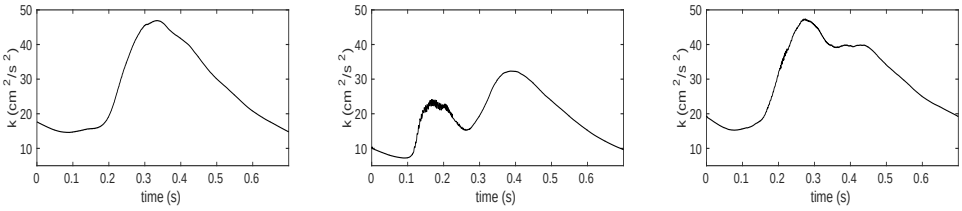

Figure 5: Global Turbulent Kinetic Energy $k(t)$ for the three patients. Left: P1; Middle: P2; Right: P3.

the *Echo-Color Doppler* (ECD) technique in [5]. Also in-vitro experiments in idealized AAA have been set up to study the presence of turbulence. In particular, we mention [2, 35], where ECD has been used to highlight the presence of turbulence in steady conditions when the Reynolds number (Re) is greater than

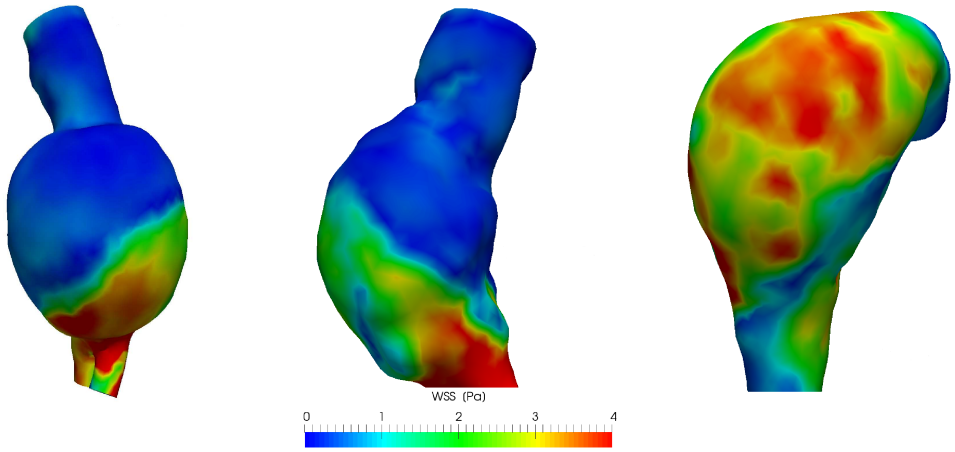

Figure 6: Peak ensemble-averaged Wall Shear Stress ($t = 0.3\,s$). Left: P1; Middle: P2; Right: P3.

2250, [12] where a *laser Doppler velocimeter* (LDV) has revealed the presence of turbulence under steady exercise conditions ($Re \simeq 4000$), and [19, 49, 36] where similar experiments highlighted that under pulsatility conditions turbulence may occur at lower Re values (peak value $Re \simeq 2300$).

The presence of turbulence effects in AAA has a great clinical impact. In the initial phases of AAA's development, turbulences interfere with endothelial cells turnover, which is at the basis of atherosclerosis development, also at relative low shear stresses [10]. This is probably due to high-frequency fluctuations and rapidly changing direction of shear stress, and to the comparable dimensions of the smallest turbulent eddies and endothelial cells. In the more advanced stages of AAA development, turbulence produces increased wall shear stresses than laminar flows, which may be responsible for further aneurysm dilatation, since the abdominal aorta regulates its diameter to maintain the shear stress below a physiological value [20]. Moreover, the increased shear stresses together with aortic wall vibration due to the large fluctuations, could damage the vessel wall, with possible implications on aneurysm growth and rupture [25, 2]. Finally, turbulent flows probably damage blood platelets promoting the formation of intraluminal thrombus (ILT) inside the aneurysmatic sac [34, 49].

4.2 Overview of computational studies

For all these reasons, some authors included the analysis of turbulence and/or transitional effects in their studies of blood dynamics in AAA. Rigid ideal geometries under steady conditions have been considered e.g. in [6, 2], where the increase of turbulent fluctuations in the distal part of the aneurysm has been reported, whereas the analysis in [19, 27] for similiar geometries and under pulsatile physiological condition revealed the formation of vortices detaching from

the wall and travelling towards the distal neck. The inclusion of the aortic wall deformation in ideal AAA geometries resulting in a fluid-structure interaction analysis has been considered for the study of turbulence effects in [26]. Studies of turbulence effects in realistic AAA geometries reconstructed by radiolgical images have been carried out in [30], where the influence of exercise conditions have been reported, and in [34], where the relationship of such effects with the thrombus formation has been highlighted.

Regarding the turbulent models included in these studies, the $k-\varepsilon$ and $k-\omega$ models were considered in [27] and [26], respectively, whereas a *Direct Numerical Simulation* was realized in [30]. A LES model implemented in a commercial software was used in [24, 23]; however no information on the LES model was provided and no analysis of turbulence was reported, the focus of these papers being the influence of boundary conditions and the monocyte deposition, respectively.

One of the major difficulties in computational models relies on a proper definition of suitable quantities capable to describe and quantify the turbulent and transitional effects in AAA. Often, the presence of such effects has been simply related to the formation of vortices and disturbed flow. However, some authors provided more statistically-sound quantities to assess turbulence in AAA. In [2], the standard deviation of the velocity field has been computed to assess and localize the presence of velocity fluctuations, whereas in [26, 30] the Turbulent Kinetic Energy has been reported as a similar quantification of turbulent instabilities.

4.3 Discussion of the methods

In this study we considered a LES model implemented in the Finite Element library LIFEV. In particular, we used the eddy viscosity $\sigma-$model. This vanishes in the cases of pure rotation, pure shear, and when the resolved scales are in axisymmetric or isotropic expansion. Moreover, the turbulent stresses decay as the distance to the solid boundary to the third power [33]. These features make the $\sigma-$model suitable to simulate fluids in enclosed domains and in presence of shear layers as happens in our case. In principle, it is suited to describe cases (like the present one) where both spatial and temporal instabilities are present. For these reasons, it has been successfully applied to describe ventricular blood fluid-dynamics [8]. Our implementation of the $\sigma-$ model has been validated in [28], where a comparison with a DNS solution highlighted the accuracy of this LES model when used in coarse meshes of stenotic carotids.

The blood has been modeled as a constant density, Newtonian, and homogeneous fluid, a well-accepted hypothesis in the previous studies of turbulence effects in AAA [26, 30, 34]. However, we observe that the Newtonian hypothesis may be considered as a limitation of the present study, since the small eddies arising as a consequence of turbulent or transitional effects may justify the use of a non-Newtonian rheology as proposed in [27]. We also assumed rigid walls,

another well accepted hypothesis in this context [27, 30, 34], which however represents in fact a second limitation of the present work. Indeed, some differences with respect to the complete fluid-structure interaction (FSI) model have been highlighted in [27]. In particular, the rigid wall assumption seems to slightly overestimate the turbulence kinetic energy. Regarding boundary conditions, in absence of measures, we prescribed a representative flow rate at the inlet, whereas zero stresses are set at the iliac outlets. The latter conditions could be justified by noticing that the resistance downstream the two iliac tracts should be equal in physiological conditions. However, the prescription of patient-specific velocity data obtained e.g. by the *phase-contrast*-MRI technology could provide more accurate results, as highlighted for AAA in [24]. Alternatively, at the outlets boundary conditions based on 3-element windkessel models may be considered, see [30] for AAA. We also observe that at the inlet we selected a priori a parabolic velocity profile to prescribe the defective flow rate condition (2). This could have an impact on the solution if the inlet region is not enough extended to allow the profile to fully develop. To overcome this drawback, Lagrange multipliers [15, 47], optimal control [17], or Nitsche [50, 48] approaches could be used to have a minor impact on the solution, see [18] for a review.

Dispite these drawbacks, in this first study on transitional effects in AAA, we decided to assume a Newtonian rheology and rigid-walls, together with simplified boundary conditions. Since the focus of the present study concerns the suitability of LES models in AAA geometries, we believe that these sources of inaccuracy should not influence the general trends and conclusions of the results we are going to discuss in the next subsection. Of course, we are working to relax them, in order to include FSI, non-Newtonian, and more-realistic boundary conditions in our future studies.

4.4 Analysis of the results

Although many authors speak about *turbulence* in AAA, here we prefer to refer to instability processes as *transition to turbulence*, since the pulsatility of the blood flow, which on the one hand is responsible for the creation of the instabilities at lower Reynolds number than in the steady case [2, 49], on the other hand does not allow the complete turbulence development. This because of the acceleration phase of a new heartbeat that laminarizes the flow [49].

From our results, we can state that transitional effects are significant in AAA, as confirmed by the large values of the standard deviation of the velocity magnitude (up to 40% of the velocity magnitude itself, see Figure 4, left). This means that flow velocity present significant random fluctuations among different heartbeats. By looking at Figures 2, 3, 4, and 5 we observe that all reported quantities related to the formation of transitional effects (i.e. the ratio between subgrid-scale and molecular viscosities, the standard deviation of the velocity magnitude, the Q-criterion, and the global KTE) are higher during the mid-deceleration phase. This confirms the previous observations reported in [49], that

at similar Reynolds numbers the flow tends to be very unstable at the beginning of the deceleration. In particular, we find that during the mid-deceleration phase, the flow jet impinges on the aneurysmatic sac creating recirculation regions around the impingement point that propagates proximally around the jet and distally through the iliac outlets. These instabilities are well captured by the distribution of the standard deviation of the velocity magnitude.

Referring to Figures 2, 3, 4, left, we observe that for all the three patients, the regions with elevated values of the subgrid-scale viscosity are in fact those of disturbed flow (high standard deviation of the velocity magnitude). This confirms the suitability of the $\sigma-$LES model in this context, being able to turn on only where and when needed, with values of the subgrid-scale viscosity reaching up to five times the molecular one. On the other hand, the LES model switches itself essentially off in the laminar regions.

As noticed by observing Figure 4, right, blood flow is characterized by a vortex ring that originates at the neck of the aneurysm, where a sudden change of diameter occurs. This ring propagates towards the inner region of the aneurysmatic sac and breaks down after the impingement. This phenomenon, at the best of our knowledge observed here for the first time in AAA, seems to be very similar to that taking place in the left ventricle and due to the passage of blood flow through the mitral valve [42, 31]. However, some differences are notable. First, the breakage of the vortex ring in AAA is due to the impingement, whereas in the heart it occurs in the middle of the ventricle chamber. This is probably due to the presence in AAA of outlets in the opposite direction of the entrance region. This, unlike the left ventricle featuring no outlets during the diastolic filling, helps the propagation of the ring towards the distal part of the sac. Moreover, as highlighted by the figures on the right ($t = 0.35\,s$), during the diastolic phase the vortex ring transforms into a swirling structure after the impingement. Again, this should be caused by the presence of the iliac outlets that favour the exit of the flow structures.

Analyzing Figure 5, we observe that the global Turbulent Kinetic Energy is clearly lower for P2 than for P1 and P3. This is also confirmed by the results reported in Table 3.2, highlighting that both k_{mean} and k_{max} decrease for P2 by more than 30%. By considering these results together with the dimensions of the aneurysms, we observe that P2 is characterized by smaller dimensions of the sac. This supports the exptected thesis that transtional effects increase with the aneurysm dimension. Thus, the synthetic indices k_{mean} and k_{max}, introduced here to quantify the transition to turbulence, could be strongly correlated with the AAA dimension. If this will be confirmed, it would provide a simple and powerful tool for clinicians to quantify transitional effects to turbulence. This deserves a particular attention for future studies.

Finally, from Figure 6 we observe that the higher values of the peak ensemble-averaged WSS are localized at the mid-deceleration phase and in the regions of the impingement, that is where transitional effects occur. These elevated values are due to the impingement itself, but probably, as observed e.g. in [20, 2, 27],

they also assume increased value with respect to the laminar case for the presence of transitional effects.

5 Conclusions

In this study we considered for the first time a large eddy simulation model to study transitional to turbulence effects in abdominal aortic aneurysms. We found that the considered LES model is able to turn itself on in regions where the instabilities and fluctuations occur, i.e. around the impingement region at the mid-deceleration phase. The transitional effects were studied by computing the standard deviation of the velocity magnitude and the Q-criterion. The latter quantity showed the formation of a vortex ring that starts from the neck of the aneurysmatic sac and propagates within this. After its breakage due to the impingement, this annular structure transforms into a swirling flow that exits through the outlets. Our results also suggested a strong correlation between the AAA dimensions and the intensity of the Turbulent Kinetic Energy.

References

[1] L. Antiga and D. Steinman. The vascular modeling toolkit (VMTK), 2009.

[2] C.L. Asbury, J.W. Ruberti, E.I. Bluth, and R.A. Peattie. Experimental investigation of steady flow in rigid models of abdominal aortic aneurysms. *Annals of Biomedical Engineering*, 23(1):29–39, 1995.

[3] E.Z. Bagci, Y. Vodovotz, T.R. Billiar, B. Ermentrout, and I. Bahar. Computational insights on the competing effects of nitric oxide in regulating apoptosis. *PLOS One*, 3(5):e2249, 2008.

[4] D. Birchall, A. Zaman, J. Hacker, G. Davies, and D. Mendelow. Analysis of haemodynamic disturbance in the atherosclerotic carotid artery using computational fluid dynamics. *European Radiology*, 16(5):1074–1083, 2006.

[5] E.I. Bluth, S.M. Murphey, L.H. Hollier, and M.A. Sullivan. Color flow doppler in the evaluation of aortic aneurysms. *Int Angiol*, (9(1)):8–10, 1990.

[6] R. Budwig, D. Elger, H. Hooper, and J. Slippy. Steady flow in abdominal aortic aneurysm models. *J Biomech Eng*, 115:418–423, 1993.

[7] S.C.P. Cheung, Kelvin K. L. Wong, Guan Heng Yeoh, William Yang, Jiyuan Tu, Richard Beare, and Thanh Phan. Experimental and numerical study on the hemodynamics of stenosed carotid bifurcation. *Australasian Physical & Engineering Sciences in Medicine*, 33(4):319–328, 2010.

[8] C. Chnafa, S. Mendez, and F. Nicoud. Image-based large-eddy simulation in a realistic left heart. *Computers & Fluids*, 94:173–187, 2014.

[9] Cantwell Chong, Perry. A general classification of three-dimensional flow fields. *Phys Fluids A*, 2:765, 1990.

[10] P.F. Davies, A. Remuzzi, E.J. Gordon, C.F. Dewey Jr, and M.A. Gimbrone Jr. Turbulent fluid shear stress induces vascular endothelial cell turnover in vitro. *Proceedings of the National Academy of Sciences of the United States of America*, 83(7):2114–2117, 1986.

[11] J.W. Deardorff. A numerical study of three-dimensional turbulent channel flow at large Reynolds numbers. *Journal of Fluid Mechanics*, 41:453–465, 1970.

[12] C.J. Egelhoff, R.S. Budwig, D.F. Elger, T.A. Khraishi, and K.H. Johansen. Model studies of the flow in abdominal aortic aneurysms during resting and exercise conditions. *Journal of Biomechanics*, 32(12):13191329, 1999.

[13] P.F. Fischer, F. Loth, S.E. Lee, S.W. Lee, D.S. Smith, and H.S. Bassiouny. Simulation of high-Reynolds number vascular flows. *Comput. Methods Appl. Mech. Engrg.*, 196:3049–3060, 2007.

[14] C. Fleming, E.P. Whitlock, T.L. Beil, and F.A. Lederle. Screening for abdominal aortic aneurysm: A best-evidence systematic review for the U.S. preventive services task force. *Ann Intern Med*, 142(3):203–211, 2005.

[15] L. Formaggia, J.F. Gerbeau, F. Nobile, and A. Quarteroni. Numerical treatment of defective boundary conditions for the Navier-Stokes equation. *SIAM Journal on Numerical Analysis*, 40(1):376–401, 2002.

[16] L. Formaggia, A. Quarteroni, and A. Veneziani (Eds.). *Cardiovascular Mathematics - Modeling and simulation of the circulatory system*. Springer-Verlag Milan, 2009.

[17] L. Formaggia, A. Veneziani, and C. Vergara. A new approach to numerical solution of defective boundary value problems in incompressible fluid dynamics. *SIAM Journal on Numerical Analysis*, 46(6):2769–2794, 2008.

[18] L. Formaggia and C. Vergara. Prescription of general defective boundary conditions in fluid-dynamics. *Milan Journal of Mathematics*, 80(2):333–350, 2012.

[19] T. Fukushima, T. Matsuzawa, and T. Homma. Cyclic transition to turbulence in rigid abdominal aortic aneurysm models. *Biorheology*, 26(2):109–130, 1988.

[20] D.P. Giddens, C.K. Zarins, and S. Glagov. Response of arteries to near-wall fluid dynamic behavior. *Applied Mechanics Reviews*, 43(5S):S98–S102, 1990.

[21] L. Grinberg, A. Yakhot, and G.E. Karniadakis. Analyzing Transient Turbulence in a Stenosed Carotid Artery by Proper Orthogonal Decomposition. *Annals of Biomedical Engineering*, 37(11):2200–2217, 2009.

[22] E. Hairer, S.P. Nørsett, and G. Wanner. *Solving ordinary differential equations: Nonstiff problems*. Springer Series in Comput. Math. Springer, 1993.

[23] D. Hardman, B.J. Doyle, S.I.K. Semple, J.M.J. Richards, D.E. Newby, W.J. Easson, and P.R. Hoskins. On the prediction of monocyte deposition in abdominal aortic aneurysms using computational fluid dynamics. *Proceedings of the Institution of Mechanical Engineers, Part H: Journal of Engineering in Medicine*, 227(10):1114–1124, 2013.

[24] D. Hardman, S.I. Semple, J.M.J. Richards, and P.R. Hoskins. Comparison of patient-specific inlet boundary conditions in the numerical modelling of blood flow in abdominal aortic aneurysm disease. *Int. J. Numer. Meth. Biomed. Engng.*, 29:165178, 2013.

[25] K. Johansen. Aneurysms. *Scientific American*, 247(1):110–125, 1982.

[26] K.M. Khanafer, J.L. Bull, and R. Berguer. Fluid-structure interaction of turbulent pulsatile flow within a flexible wall axisymmetric aortic aneurysm model. *European Journal of Mechanics - B/Fluids*, 28(1):88–102, 2009.

[27] K.M. Khanafer, J.L. Bull, G.R. Upchurch Jr., and R. Berguer. Turbulence significantly increases pressure and fluid shear stress in an aortic aneurysm model under resting and exercise flow conditions. *Annals of Vascular Surgery*, 21(1):67–74, 2007.

[28] R.M. Lancellotti, C. Vergara, L. Valdettaro, S. Bose, and A. Quarteroni. Large eddy simulations for blood fluid-dynamics in real stenotic carotids. MOX-Report n. 63-2015, Department of Mathematics, Politecnico di Milano, Italy, 2015.

[29] S.E. Lee, S.W. Lee, P.F. Fischer, H.S. Bassiouny, and F. Loth. Direct numerical simulation of transitional flow in a stenosed carotid bifurcation. *J Biomech*, 41(11):2551–2561, 2008.

[30] A.S. Les, S.C. Shadden, C.A. Figueroa, J.M. Park, M.M. Tedesco, R.J. Herfkens, R.L. Dalman, and C.A. Taylor. Quantification of hemodynamics in abdominal aortic aneurysms during rest and exercise using magnetic resonance imaging and computational fluid dynamics. *Annals of Biomedical Engineering*, 38(4):12881313, 2010.

[31] R. Mittal, J.H. Seo, V. Vedula, Y.J. Choi, H. Liu, H.H. Huang, S. Jain, L. Younes, T. Abraham, and R.T. George. Computational modeling of cardiac hemodynamics: Current status and future outlook. *Journal of Computational Physics*, 305:1065–1082, 2016.

[32] U. Morbiducci, R. Ponzini, G. Rizzo, M. Cadioli, A. Esposito, F.M. Montevecchi, and A. Redaelli. Mechanistic insight into the physiological relevance of helical blood flow in the human aorta: an in vivo study. *Biomechanics and Modeling in Mechanobiology*, 10(3):339355, 2011.

[33] F. Nicoud, H. Baya Toda, O. Cabrit, S. Bose, and J. Lee. Using singular values to build a subgrid-scale model for large eddy simulations. *Physics of Fluids*, 23(8):085106, 2011.

[34] M.J. O'Rourke, J.P. McCullough, and S. Kelly. An investigation of the relationship between hemodynamics and thrombus deposition within patient-specific models of abdominal aortic aneurysm. *Proceedings of the Institution of Mechanical Engineers, Part H: Journal of Engineering in Medicine*, 226(7):548–564, 2012.

[35] R.A. Peattie, C.L. Asbury, E.I. Bluth, and J.W. Ruberti. Steady flow in models of abdominal aortic aneurysms. part i: Investigation of the velocity patterns. *J Ultrasound Med*, 15(10):679–688, 1996.

[36] R.A. Peattie, T.J. Riehle, and E.I. Bluth. Pulsatile flow in fusiform models of abdominal aortic aneurysms: Flow fields, velocity patterns and flow-induced wall stresses. *J Biomech Eng*, 126(4):438–446, 2004.

[37] M. Piccinelli, C. Vergara, L. Antiga, L. Forzenigo, P. Biondetti, and M. Domanin. Impact of hemodynamics on lumen boundary displacements in abdominal aortic aneurysms by means of dynamic computed tomography and computational fluid dynamics. *Biomech Model Mechanobiol*, 12(6):1263–1276, 2013.

[38] S.B. Pope. *Turbulent flows*. Cambridge University Press, 2000.

[39] A. Quarteroni and A. Valli. *Numerical approximation of partial differential equations*. Springer, 1994.

[40] V.L. Rayz, S.A. Berger, and D. Saloner. Transitional flows in arterial fluid dynamics. *Computer Methods in Applied Mechanics and Engineering*, 196(31–32):3043–3048, 2007.

[41] R.S. Rogallo and P. Moin. Numerical Simulation of Turbulent Flows. *Annual Review of Fluid Mechanics*, 16:99–137, 1984.

[42] J.H. Seo, V. Vedula, T. Abraham, A.C. Lardo, F. Dawoud, H. Luo, and R. Mittal. Effect of the mitral valve on diastolic flow patterns. *Physics of fluids*, 26(12):121901, 2014.

[43] J. Smagorinsky. General circulation experiments with the primitive equations: I. The basic experiment. *Monthly weather review*, 91:99–164, 1963.

[44] J.S. Stroud, S.A. Berger, and D. Saloner. Numerical Analysis of Flow Through a Severely Stenotic Carotid Artery Bifurcation. *J Biomech Eng*, 124(1):9–20, 2002.

[45] F.P. Tan, G. Soloperto, S. Bashford, N.B. Wood, S. Thom, A. Hughes, and X.Y. Xu. Analysis of Flow Disturbance in a Stenosed Carotid Artery Bifurcation Using Two-Equation Transitional and Turbulence Models. *J Biomech Eng*, 130(6):061008, 2008.

[46] T.E. Tezduyar. Stabilized finite element formulations for incompressible flow computations. *Advances in Applied Mathematics*, 28:1–44, 1992.

[47] A. Veneziani and C. Vergara. Flow rate defective boundary conditions in haemodinamics simulations. *International Journal for Numerical Methods in Fluids*, 47:803–816, 2005.

[48] C. Vergara. Nitsche's method for defective boundary value problems in incompressibile fluid-dynamics. *J Sci Comp*, 46(1):100–123, 2011.

[49] T.H. Yip and S.C.M. Yu. Cyclic transition to turbulence in rigid abdominal aortic aneurysm models. *Fluid Dynamics Research*, 29(2):81–113, 2001.

[50] P. Zunino. Numerical approximation of incompressible flows with net flux defective boundary conditions by means of penalty technique. *Computer Methods in Applied Mechanics and Engineering*, 198(37-40):3026–3038, 2009.

MOX Technical Reports, last issues

Dipartimento di Matematica
Politecnico di Milano, Via Bonardi 9 - 20133 Milano (Italy)

52/2016 Paolucci, R.; Evangelista, L.; Mazzieri, I.; Schiappapietra, E.
The 3D Numerical Simulation of Near-Source Ground Motion during the Marsica Earthquake, Central Italy, 100 years later

53/2016 Antonietti, P. F.; Manzini, G.; Verani, M.
The fully nonconforming Virtual Element method for biharmonic problems

51/2016 Guzzetti, S.; Perotto, S.; Veneziani, A.
Hierarchical Model Reduction for Incompressible Flows in Cylindrical Domains: The Axisymmetric Case

48/2016 Scardulla, S.; Pasta, S.; D'Acquisto, L.; Sciacca, S.; Agnese, V.; Vergara, C.; Quarteroni, A.; C
Shear Stress Alterations in the Celiac Trunk of Patients with Continuous-Flow Left Ventricular Assist Device by In-Silico and In-Vitro Flow Analysis

49/2016 Formaggia, L.; Scotti, A.; Sottocasa, F.
ANALYSIS OF A MIMETIC FINITE DIFFERENCE APPROXIMATION OF FLOWS IN FRACTURED POROUS MEDIA

50/2016 Ambrosi, D.; Pezzuto, S.; Riccobelli, D.; Stylianopoulos, T.; Ciarletta, P.
Solid tumors are poroelastic solids with a chemo--mechanical feedback on growth

46/2016 Lila, E.; Aston, J.A.D.; Sangalli, L.M.
Smooth Principal Component Analysis over two-dimensional manifolds with an application to Neuroimaging

47/2016 Canuto, C.; Nochetto, R. H.; Stevenson R.; Verani, M.
On p-Robust Saturation for hp-AFEM

42/2016 Iannetti, L.; D'Urso, G.; Conoscenti, G.; Cutri, E.; Tuan, R.S.; Raimondi, M.T.; Gottardi, R.; Zu
Distributed and lumped parameter models for the characterization of high throughput bioreactors

43/2016 Ambrosi, D.; Ciarletta, P.; De Falco, C.; Taffetani, M.; Zunino, P.
A multiscale modeling approach to transport of nano-constructs in biological tissues